Instrument Science Report WFC3 2012-09

WFC3 UVIS Charge Transfer Efficiency October 2009 to October 2011

K. Noeske, S. Baggett, H. Bushouse, L. Petro,
R. Gilliland, V. Khozurina-Platais

June 9, 2012

Abstract Using observations of calibration fields in the star clusters NGC6791 and NGC104/47 Tuc, we have investigated the evolution of the charge transfer efficiency (CTE) of the WFC3/UVIS detectors over a 2-year period starting 5 months after the WFC3 installation, ranging from October 2009 to October 2011. We find a strong evolution of the CTE, amounting to more than 0.1 mag CTE loss per year for stars with a total flux of 1000 electrons, at large distances from the readout amplifiers, in short-exposure zero sky background images. These maximum possible CTE losses for such stars have reached 0.3 mag (24%) as of October 2011 in 3-pixel radius apertures. For even fainter stars around 300 electrons, these losses can reach 50%.

The CTE degradation and associated losses decrease for increasing source fluxes, and for higher sky background levels which partially fill the detector charge traps during readout. Already a low background of 2-3 electrons per pixel significantly lowers CTE losses, while a 20-30 electron per pixel background in longer-exposure broadband images brings CTE losses to few percent for sources ranging from few 100 to 10s of 1000s of electrons. For faint sources on near-zero sky backgrounds, we also see significantly lower CTE losses in longer (approx. 350 seconds) exposures than in shorter ones (30-60 seconds). This most likely reflects that the larger total charge collected in longer images has a similar, yet non-uniformly distributed trap-filling effect as a higher sky background.

We present an empirical polynomial model that corrects CTE losses for point source aperture photometry as a function of observation date, source flux, and source distance on the detector from the readout amplifiers. The model coefficients are given for low and high backgrounds and long and short exposures separately, while we collect further calibration data to include a smooth parameterization of the latter parameters.

1. Introduction: UVIS CTE Evolution

Like all CCD detectors in low-Earth orbit, the WFC3/UVIS CCDs experience a degradation of their Charge Transfer Efficiency over time, introduced by their exposure to energetic radiation. Most severely during passages through the South Atlantic Anomaly, energetic protons leave defects in the detector's crystal lattice that manifest themselves as charge traps.

During readout, as the charge package in each pixel is shifted along columns toward the amplifiers, the charge traps in the detector lattice capture electrons from this charge package. This captured charge is subsequently released from the traps in a stochastical manner on a variety of timescales. Some of these timescales are longer than the time between row-to-row charge shifts in the UVIS CCDs ($\sim$ 40 milliseconds). Part of the charge captured from the pixel is therefore released into pixels that are subsequently shifted across the charge trap, i.e. in rows further away from the amplifiers. This process leads to a loss of charge in pixels that carry significant charge above their local average, and to a charge trail that points away from the amplifiers and declines in intensity with increasing distance from the source.

The resulting Charge Transfer Inefficiency (CTI) is a function of the observing date, as the number of charge traps per pixel increases with time. The charge lost from a source also depends on the number of traps it has to pass during readout, i.e. its distance in detector rows from the amplifiers or detector Y coordinate. In addition, the CTI losses are a function of the source flux; while the number of electrons captured in a trap depends on the amount of charge in the pixel charge package (Anderson & Bedin 2010), the dependence is very non-linear and faint pixels lose a much larger fraction of their charge to CTI than very bright pixels. To complicate matters further, the charge lost to each pixel depends on the charge in the pixels at row numbers closer to the amplifier: the charge in these preceding pixels will partially pre-fill charge traps, lowering the losses of subsequent passing pixels. The CTI losses hence depend on the intensity distribution of a source, the density of sources in a field, and the total background from sky and instrument emission collected during the exposure.

To measure and correct CTI , the WFC3 team has conducted both external observations of star fields and internal calibration exposures. Recent results are published in

- the WFC3 UVIS CTE Whitepaper (Baggett et al. 2011), `http://www.stsci.edu/hst/wfc3/ins_performance/CTE/cte.pdf`,
- ISR-WFC3-2011-02 (*WFC3/UVIS Charge Injection Behavior: Results of an Initial Test*, Bushouse et al. 2011, `http://www.stsci.edu/hst/wfc3/documents/ISRs/WFC3-2011-02.pdf`),
- ISR-WFC3-2011-06 (*WFC3/UVIS CTE External Monitoring in Cycle 17*, Khozurina-Platais et al., `http://www.stsci.edu/hst/wfc3/documents/ISRs/WFC3-2011-06.pdf`),
- the *Cycle 19 Update Document on CTE and Charge Injection* (Noeske et al. 2011, `http://www.stsci.edu/hst/wfc3/ins_performance/CTE/UVIS_CTE_Cy19_Update.pdf`),
- and the UVIS CTE website: (`http://www.stsci.edu/hst/wfc3/ins_performance/CTE/`) .

Results presented in these documents showed that in the absence of sky background, which is the worst case, moderately faint (500 - 2000 electrons) stars at detector Y coordinates far from the readout amplifiers

can experience flux losses approaching 10% in small (r=3 pixel) apertures, as of March 2011. Losses are lower for brighter targets and/or images with higher sky backgrounds: for a background level of 20-30 electrons per pixel, CTE losses for the aforementioned stars (500 to 2000 electrons) are only $\sim 2\%$. Stars with 2000-4000 and 8000-16000 electrons in images with essentially zero background show losses of $\sim 4 \pm 2\%$ and $2 \pm 2\%$, respectively.

The initial decline of the UVIS CTE was steeper than observed in, e.g., the ACS detectors during their first two years of on-orbit time. The suspected reason is the extreme solar activity minimum during UVIS' initial two years of flight, which causes a *higher* incidence of damaging radiation (Fürst et al. 2009). This idea is supported by the evolution of the ACS CTE, which seems to have experienced an unusually steep decline during the recent solar activity minimum (Chiaberge et al. 2009, Massey 2010). If this scenario is correct, then the CTE degradation of HST's CCD detectors should now slow down with the increase in solar activity and decrease in energetic protons.

In this document, we present the results of the external observations of star clusters that sample a wide range of source fluxes, different source densities and background levels, spaced typically 4 months apart to measure its time dependence. We analyze observations of star clusters over the first two years of the WFC3 on-orbit time with a focus on the evolution of the UVIS CTE as a function of source flux, detector Y position, for very low and for moderate backgrounds.

Results on the CTE evolution are intended to allow observers to estimate CTE losses for their future observation dates when designing UVIS observations, and to consider whether the observations can benefit from measures that moderate CTE, such as placing the target at row numbers close to the amplifier, or applying Charge Injection (see Baggett et al. 2010). Future CTE mitigation options may include a post-flash. Preliminary models of the traps in WFC3 show that, for faint sources, a relatively small level of background (10-20e^-) may provide a significant mitigation of CTI (Anderson, priv.comm.). In such situations, the benefit of a low-level post-flash may outweigh the noise penalty incurred. As a consequence, recent work has focused on reinstating the post-flash capability on WFC3, a mode initially retired during ground testing in favor of the low-noise charge injection capability (Giavalisco, 2003). Post-flash engineering tests have commenced in spring 2012 with results and advice for observers expected over the summer.

Furthermore, we use these data to provide an empirical CTI correction for point source aperture photometry, as a function of observation date, detector Y position, and source flux, for low and moderate backgrounds. A pixel-based reconstruction algorithm for CTI-affected UVIS images is currently being developed, adapted from the ACS CTI correction described in Anderson & Bedin 2010.

Updates on the status of the UVIS CTE, the empirical correction model and the pixel based correction will be published on the UVIS CTE webpage, `http://www.stsci.edu/hst/wfc3/ins_performance/CTE/`.

2. Observations and Data Analysis

Data presented in this document were obtained during the Cycle 17, 18 and 19 calibration programs CAL/WFC3 11924 (Platais et al.), 12348 (Baggett et al.), and 12379 and 12692 (Noeske et al.). The observation dates cover a period of 749 days starting four and a half months after the May 2009 installation of WFC3; individual epochs were observed on 2 Oct 2009 (MJD 55106), 25 Mar 2010 (MJD 55280), 2 Sep 2010 (MJD 55441), 17 Nov 2010 (MJD 55517), 9 Mar 2011 (MJD 55629), and 20 Oct 2011 (MJD 55854).

While UVIS CTE monitoring up to Cycle 17 was performed in a calibration field in NGC 6791, from Cycle 18 on we included a second target, a calibration field in 47 Tuc (NGC 104). The NGC 104 field, offset from the cluster center, has a higher surface density of stars than NGC 6791, allowing us to study the effect of source density on the CTE. A higher density of sources should provide more charge that can pre-fill the electron traps during the readout, and is expected to moderate CTE losses in a similar, but less homogeneous way than a higher background signal would. While the lower source density of NGC 6791 should yield a more "pure" CTE measurement , star counts in certain flux bins have been found to be relatively sparse, so the higher source density in 47 Tuc also improves on the statistical significance of the data.

To probe CTE in different sky backgrounds, these observations were performed in both a narrow band and a broad band filter, F502N and F606W. We furthermore obtained both long (348 to 420 sec) and short (30 or 60 sec) exposures in each filter. Resulting backgrounds are practically zero in the F502N images, and 2-3 and 20-30 electrons per pixel in the short and long F606W images, respectively.

The observing technique we employ to measure the CTE is illustrated in Figure 1. A problem of CTE measurements is the lack of reference fluxes that are unaffected by CTE losses. Such fluxes would need to be observed with the same instrument and an identical detector that has pristine, 100% CTE. Such data are of course unavailable: Even data taken shortly after launch are not suitable for that purpose because CTE is never 100%. Instead, we use the dependence of the CTE on the detector row number (detector Y coordinate). A source on the row next to the readout amplifier will practically not pass any charge traps during readout, except for any traps in the serial register. A source at the opposite side of the detector will experience the loss of passing 2048 pixel rows occupied by charge traps. Our observing pattern takes two images of the calibration starfield, offset from each other by approximately 2000 pixels in detector Y coordinate, such that the stars that were observed on the UVIS2 detector (lower detector in Fig. 1) are then observed on the UVIS1 detector (upper detector in Figure 1). Because the amplifiers are located on opposing sides of both detectors, this procedure places stars at different distances to the readout amplifiers: A star Y rows from the amplifiers on the UVIS1 detector will be located at (2048-Y) rows from the amplifiers on the UVIS2 detector. Stars close to rows 1 and 2048 experience practically no CTE loss one detector and maximal CTE loss on the other.

Our plots, and earlier studies of CTE on UVIS, show that the logarithm of the CTE losses is very linear with detector row number Y, i.e. linear losses are in good approximation an exponential function of detector row number. A logarithmic plot (in our case, we show magnitudes) of the star flux ratios observed on both detectors, vs the row number of one detector, then shows :

$$-2.5 \log \frac{f_1}{f_2} = -2.5 \log \frac{f_0 e^{-cY}}{f_0 e^{-c(2048-Y)}} = -2.5c(2048 - 2Y) \quad (1)$$

where f_0 is the star flux unaffected by CTE. The resulting slope in Figure 2 is hence **twice** the slope of the CTE loss in magnitudes as a function of detector row number.

An obvious downside of this method is that it does not yield the CTE for both individual detectors, but mixes the CTE of both detectors. CTE differences of individual detectors can be estimated from the flux ratio of stars in long and short exposures (UVIS CTE Whitepaper, http://www.stsci.edu/hst/wfc3/ins_ performance/CTE/cte.pdf). However, this method does not provide an absolute CTE measurement. Although the flux of the star in long exposures that is used for reference is less affected by CTE losses than the star's lower flux in short exposures, CTE losses are typically non-zero even in long exposures, except for very high

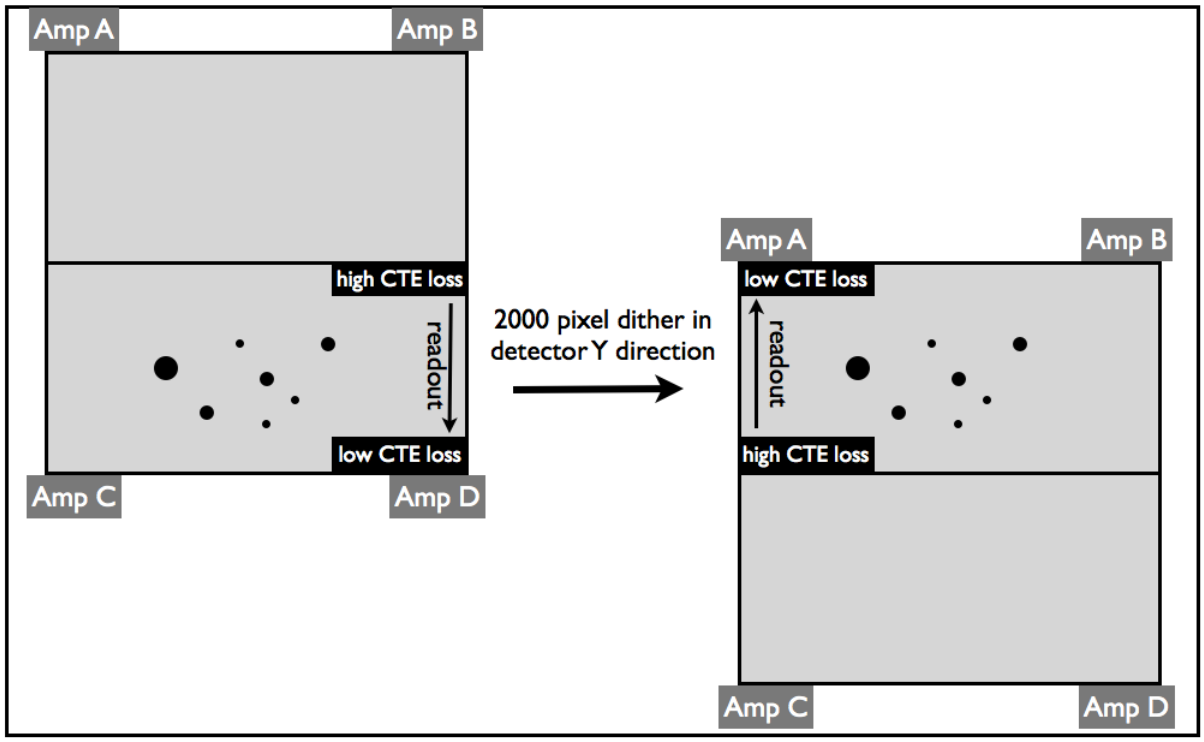

Fig. 1.— Observing technique for the CTE measurements. Observations were repeated with a 2000 pixel dither step in the detector POS-TARG Y direction, such that the sky area that first fell onto the UVIS2 detector was imaged again on the UVIS1 detector. Because the read-out amplifiers are on opposite ends of UVIS1 (amplifiers A B) and UVIS2 (amplifiers C D), stars that were near the amplifier (low row number) in the UVIS2 image are far from the amplifier in UVIS1 and vice versa. The ratio of the fluxes of stars from both images, plotted as a function of the row number (detector Y), hence measures the absolute amount of CTE losses. See Figure 2 for examples.

fluxes. This non-zero CTE in the long exposures leads to a CTE loss measurement that underestimates the actual losses when the long-short exposure comparison method is used. We show here the former method, giving an absolute CTE measurement of CTE losses. From tests with an independent dataset of stellar photometry, we find that measurements mixing both detectors are in fact suitable to correct CTE-affected data on either detector.

It is, in principle, possible to obtain an absolute CTE measurement for both detectors individually, if the same star field is observed on each detector twice, at a 180 degree rotated orientation. Because CTE evolves, these exposures would have to be taken with a short time separation, days to weeks. For HST, this is only possible for targets close to the anti-Sun direction, in very short scheduling windows. These constraints are due to power requirements, put in place to keep the solar arrays oriented to the sun to provide sufficient power to the spacecraft. We are currently testing such a calibration technique in Cycle 19.

Photometry of the stars was performed using DAOPHOT under IRAF in aperture radii of 3 pixels, with sky annuli with an inner radius of 10 pixels and a width of 10 pixels. Images on which the photometry was measured were calibrated through CALWF3 as integrated into the HST archive. These calibrated FLT images are corrected for bias, dark current and flat fields, but are not corrected for geometric distortion. Prior to performing photometry, the FLT images were therefore corrected with the appropriate pixel area maps [1], and the stars' detector coordinates returned by DAOPHOT were corrected for geometric distortion. Stars were cross-identified between both detectors, using a closest-coordinate matching and rejecting matches with a maximum distance $\sqrt{\Delta_X^2 + \Delta_Y^2} > 5$ pixels. We also rejected stars that had multiple matches within a radius of 4 pixels to avoid blended sources.

The ratios of the fluxes between UVIS1 and 2 (expressed in magnitudes) are shown as a function of the detector Y coordinate (row number) of UVIS2, for different observation setups, in the example CTE plots in Figure 2.

Our analysis only includes stars with a formal photometric error of < 0.1 mag in individual images. To reject stars in individual exposures that were affected by cosmic rays or image artifacts, we compared star fluxes in pairs of dithered (few pixels) exposures that were taken on the same side of the large 2000 pixel Y dither throw. We removed stars that in the image pairs dithered by few pixels showed flux differences > 2 times the formal photometric error of that star. For the majority of the data, each pointing has however only a single image; cosmic rays are therefore a concern and increase photometric scatter. As is evident from comparing the short (left) and long (right) exposure panels in Figure 2, this is especially true in long exposure images where the area density of cosmic rays is higher. In future updates of UVIS CTE measurements, we will remove affected stars with a cosmic ray identification algorithm. Scatter from cosmic rays affecting the aperture photometry is a primary source of uncertainties in the measurements of the CTE slopes for fainter stars (our flux bins of 500 to 2000 electrons and below) because the sources' intrinsic photometric errors introduce significant scatter. The problem is most pronounced for the sparse stellar cluster NGC 6791 where each flux bin contains a smaller number of stars.

For each combination of target, date of observation, filter, and integration time, the CTE slope was determined through an outlier-resistant linear fit algorithm (ROBUST_ LINEFIT, IDL Astronomy User's Library), treating the CTE-induced magnitude differences as independent variables. The resulting CTE slope measurements are shown as lines in Fig. 2. Note that the plots display twice the amount of CTE losses

[1] `http://www.stsci.edu/hst/wfc3/pam/pixel_area_maps`

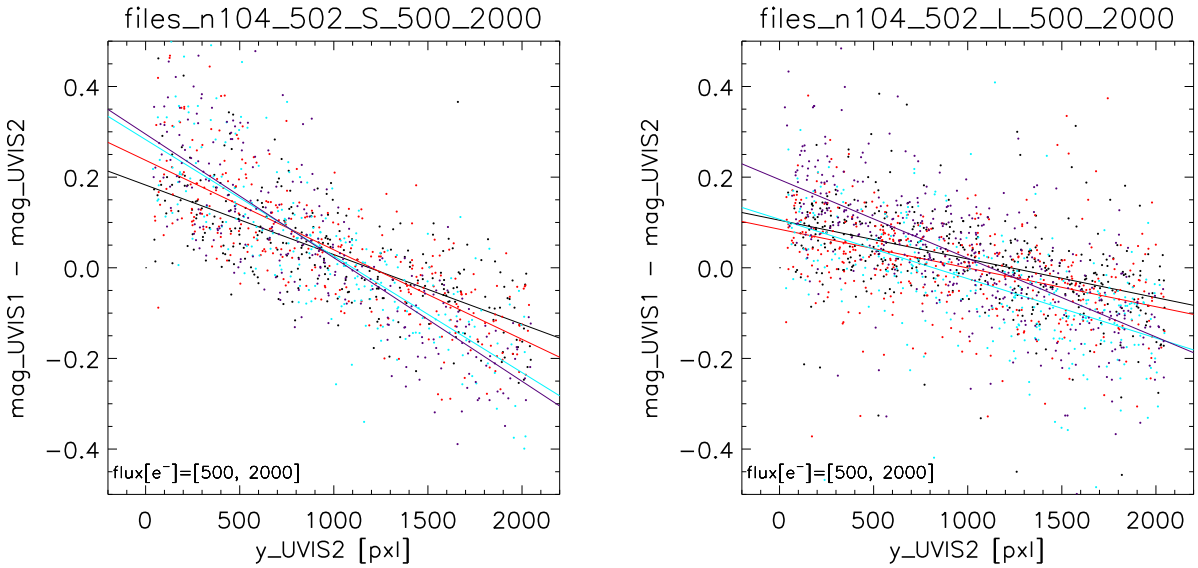

Fig. 2.— CTE in F502N images of NGC104/47Tuc, in short (30-60 sec, left) and long ($\sim$ 360 sec, right) exposures. Both panels show stars that accumulate 500 to 2000 electrons over the total exposure time of the image. Colors of the dots and linear fits correspond to the MJD of the observations: black, red, cyan and purple refer to MJDs of 55441 (2 Sep 2010), 55517 (17 Nov 2010), 55629 (9 Mar 2011) and 55854 (20 Oct 2011), respectively. Note that the plots display twice the amount of CTE losses across each detector.

across each detector, as discussed above.

3. UVIS CTE evolution from October 2009 to October 2011

Figure 3 displays the UVIS CTE evolution over 2 years. The Y axis shows the slopes of CTE in magnitudes per 2048 detector rows, for stars in different flux bins from fainter (highest CTE losses, black symbols) to brighter (lowest CTE losses, blue symbols). The relatively large error bars on the CTE slopes for some of the NGC6791 data (top right panel) stem from the photometry artifacts due to cosmic rays in long exposures and the relatively sparse number of sources in that cluster, as discussed in the previous section.

Brighter sources have lower relative flux losses, reflecting that CTE losses are limited by a finite number of charge traps in the detector . The number of electrons lost from a source will be a non-linear function of the source flux and intensity distribution (Sect. 1). However, Figure 3 suggests that the CTE loss for stars far from the amplifier in all three flux bins is of the order of 1-2x10^2 electrons in low backgrounds for the most recent epoch (October 2011). Note that in low backgrounds, CTE effects remain significant (formal fit errors) for stars up to the 8000 to 32000 electron bin up to a few percent .

CTE losses for fainter sources can be inferred from Figure 4 where we plot the CTE slope (loss in magnitudes per 2048 detector rows) against source flux, for our range of observed modified Julian dates (black symbols, lowest losses: earliest to blue symbols, highest losses: most recent). For the lowest background and shortest exposures (F502N, top left panel), where CTI losses will be most dramatic, sources with $\sim 300\,e^-$ can lose up to $\sim$ 0.45 mag (34%) of their flux; extrapolating the fitted curve (blue line) to lower fluxes suggests that losses for a $100\,e^-$ star may exceed 50% of its flux in a 3 pixel radius aperture in the most recent (October 2011) data.

CTE clearly decreases over time in all backgrounds and wherever the CTI losses show a significant trend over time within the slope measurement errors. From the model fits shown in Figure 4, we see that in short exposures and zero backgrounds (top left panel), the CTI loss per 2048 detector rows for a $\sim 1000\,e^-$ star in a 3 pixel radius aperture rises from 0.06 to 0.3 mag between the MJD 55106 and 55854. This increase in CTE slope over 749 days or 2.05 years suggests an increase of 0.12 mag of loss per 2048 detector rows. For brighter sources, higher background levels or exposures (see below), the relative increase of CTI losses are lower, down to few 1/100 of a magnitude per year for $10,000e^-$ stars or for sources in high $(20-30\,e^-)$ backgrounds (bottom right panel).

The most recent data points (October 2011, MJD 55854) in some panels of Figure 3 suggest that the initial decline of the UVIS CTE may have started to slow down, as would be expected from the increase of solar activity since the extended minimum at the time of the WFC3 installation in May 2009. By the time the latest data shown in this document were taken, the solar radio flux at 10.7 cm had risen from its 2009 minimum to about the halfway level between the 2009 minimum and the preceding 2002 maximum (`http://www.swpc.noaa.gov/SolarCycle/`). The solar activity as measured by the 10.7 cm radio flux is known to be inversely correlated with the radiation intensity in the South Atlantic Anomaly (SAA) (Fürst et al. 2009, Casadio et al. 2011), the zone of intense radiation where most of the UVIS detector damage is thought to occur. As outlined in Fürst et al. (2009), during higher solar activity, heating of the upper atmosphere increases the neutral atmospheric density in the altitude range of the SAA, and provides enhanced shielding (through absorption and deflection) against trapped particles. The data presented by Fürst et al.

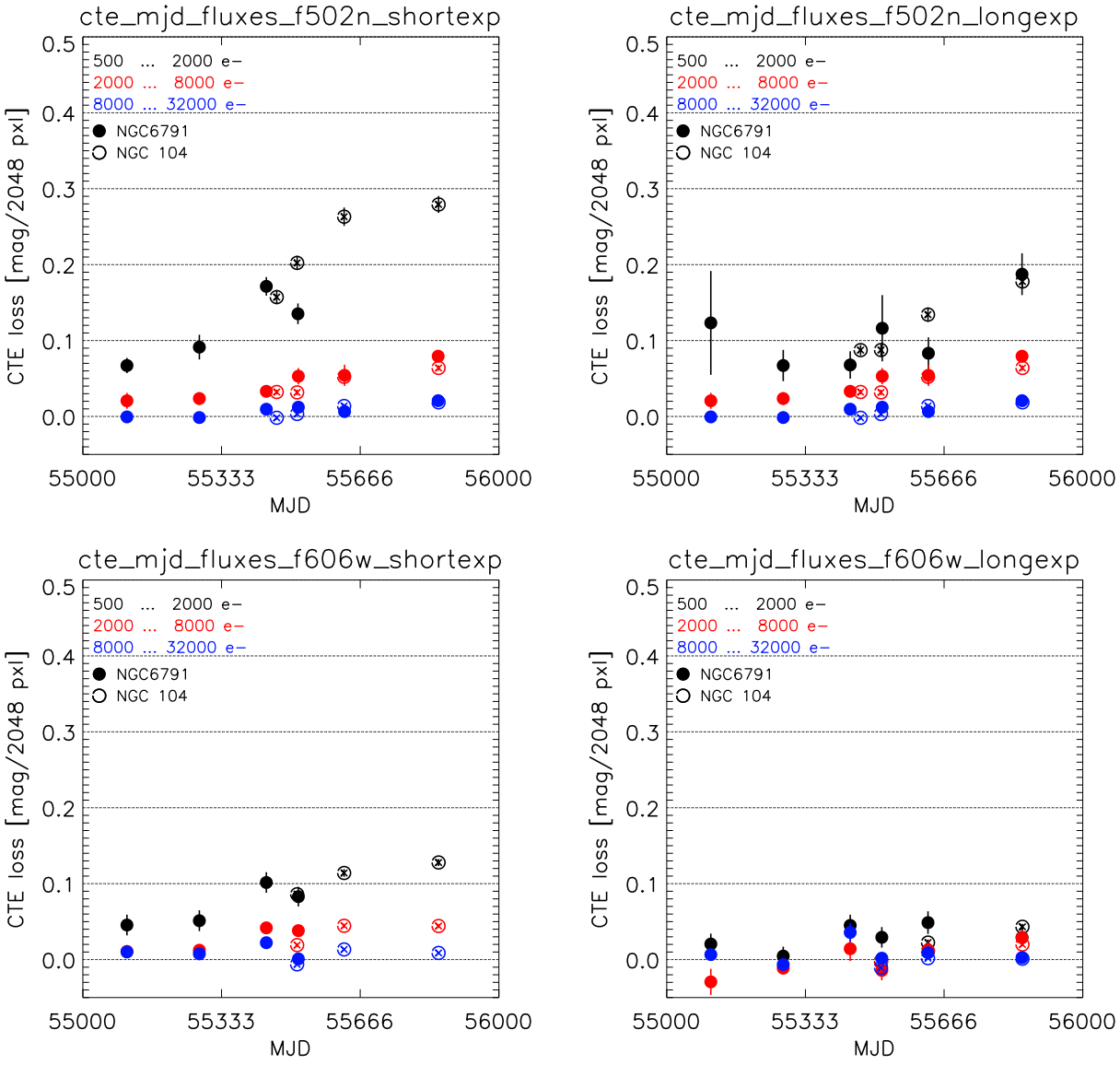

Fig. 3.— UVIS CTE evolution between October 2009 and October 2011, for stellar aperture photometry within 3 pixel radius apertures. Panels show the CTE loss slope in magnitudes per 2048 detector rows, taken from fits such as those shown in the examples in Figure 2, as a function of observing date, given in MJD. Panels on the left and right hand side side refer to short and long exposures, respectively. Top row: F502N narrow band exposures (zero background in both short and long exposures). Bottom row: F606W broad band exposures (background $2-3$ and $20-30e^{-1}$ in short and long exposures, respectively) . The colors of the symbols indicate stars in different flux ranges, given in the panels. Closed and open symbols refer to data from the sparse cluster NGC 6791 and the denser field in NGC 104/47 Tuc, respectively.

(2009) show, however, a time delay of 1 year in this inverse correlation, such that the decrease of the SAA particle flux is lagging behind the increase of solar activity, and vice versa. In view of these results, the CTE evolution as of October 2011 should only reflect the mild increase of solar activity seen in the solar radio flux and sunspot counts by October 2010. An at most mild trend for a decelerating CTE decrease in our data, which needs to be treated with caution since it is based on a single epoch only, would hence be expected. We expect to see benefits of increasing solar activity only in the forthcoming 2012 epochs of our CTE calibration data, which will be published as an update as we complete their analysis during the course of 2012.

4. Effect of background level, source density and exposure duration

A comparison of the panels in Figures 3 and 4 illustrates that even a small amount of sky background is very effective at lowering CTI losses in UVIS data. The top left panels in both figures represent the worst-case scenario of CTI losses, short exposures (30-60 seconds) with zero background (F502N narrowband data). CTI losses in the bottom left panel, showing data for short exposures in the F606W broad band filter are significantly lower, roughly one half of the loss in magnitudes displayed by the zero background narrow band data in the top left panels, for stars in the 500 to 2000 electron flux bin. The short exposure time F606W data have very modest backgrounds of 2-3 electrons per pixel, and show that even small background levels that do not contribute much additional Poisson noise to the images are effective at partially occupying the electron traps, which then will inflict much lower damage on the science sources. The promise of significant CTE mitigation using small levels of background is the prime motivation for reviving the post-flash capability on WFC3. Details of the development and possible availability of this mode in the future will be posted on the WFC3 CTE page (`http://www.stsci.edu/hst/wfc3/ins_performance/CTE/`) as well as announced on the main WFC3 page, the electronic newsletter, and in the Astronomer's Proposal Tool (APT) proposal instructions.

Background levels more typical for long exposure broad band exposures are displayed in the bottom right panels of Figures 3 and 4. The exposure times ranged from 348 to 360 seconds in the F606W filter, in the lower range of what observers typically use in individual long broad band exposures. The resulting sky background levels range between 20 and 30 electrons per pixel across these images, and will be accordingly higher in longer science exposures. However, even the 20-30 electrons per pixel backgrounds strongly suppress - yet do not eliminate - CTI losses across a wide range of source fluxes, down to few 1/100 of a magnitude (few percent), compared to several 1/10 of a magnitude (few 10s of percent) of CTI losses seen in zero background exposures.

The density of sources in the calibration field should have a non-negligible effect, since sources passing across electron traps during the detector readout process should partially fill these traps and lower CTI losses for sources that subsequently pass the same traps. A comparison of the sparse field NGC6791 (filled symbols) and denser field in NGC104/47 Tuc (open symbols) in the panels of Figure 3 and 4 shows a mild tendency for the denser field (open symbols) to experience smaller CTI losses, but these are usually within the uncertainties of individual CTE slope measurements. The trend is mostly seen for brighter stars where CTI slope measurement errors are smaller, and we currently only have a few epochs with data for both calibration fields. We have only started to observe both fields simultaneously halfway through the calibration program, and some epochs shown in Fig 3 stem from a specialized program (12348) that was not part of the standard CTE monitoring and did not observe both fields. In addition, the source density in the

denser field, on average 2-3x that of the sparse field, varied between epochs because the epoch-dependent different sky orientations of the 47 Tuc calibration field sample varying parts of the steep density gradient in 47 Tuc. The 2012 CTE monitoring program (program ID 12692, Noeske et al.) includes an improved sampling of field source density, and we will present a quantitative analysis of an, apparently modest, source density dependence of the CTI losses in a future update.

The effects of the exposure duration, on the other hand, are significant. The top row panels in Figures 3 and 4 show that faint sources in short exposures, 30-60 seconds, experience significantly higher CTI losses than in long exposures (348-360 seconds) in the top right panels. Both these long and short F502N images have practically zero background. Note that we do not compare CTI losses of the same stars that would in different exposure times accumulate different total fluxes and hence naturally experience lower CTI losses in long exposures. Instead, the comparison is between different stars with equal total observed fluxes - intrinsically brighter stars that in short exposures accumulate the same total electron fluxes as intrinsically fainter stars in long exposures. We attribute the more moderate CTI losses in longer exposures to the larger total flux accumulated in the image in longer exposures - both from science sources and from cosmic ray events. The effect of this additional charge in longer exposure images is expected to be similar to that of an irregularly distributed background - charge accumulated in detector rows closer to the amplifiers will, during readout, pass over charge traps and partially occupy them, moderating CTI losses to charge traps for sources at rows more distant from the amplifier that subsequently passes the same traps during the readout process.

5. Empirical correction model

As outlined throughout this document, the CTI losses are a strong function of the observation date, source flux, image background level, and the source distance from the amplifier.

We have seen before that the CTE slopes, representing CTI losses vs detector row number from the amplifier, are in very good approximation linear with detector row number if expressed in magnitudes (see Figure 2). It is therefore convenient to treat the source distance as a single number, the CTE slope S in magnitudes per 2048 detector rows, as is shown in Figure 4.

The data in Figure 4 suggest that at any given epoch, the dependence of the CTE slope S on the logarithmic source flux is a smooth monotonic function that can be well approximated by a 2nd degree polynomial, and that these 2nd degree polynomials vary in a smooth monotonic manner with the observation date. We hence attempted to fit the CTE slope S as a 2nd degree bivariate polynomial function of the source flux and observation date, with good success, as can be seen from the model curves overplotted in Figure 4:

$$S = \sum_{i,j=0}^{2} c_{ij} d^i f^j \tag{2}$$

or, written out,

$$S = c_{00} + c_{01}d + c_{02}d^2 + c_{10}f + c_{11}df + c_{12}d^2f + c_{20}f^2 + c_{21}df^2 + c_{22}d^2f^2 \tag{3}$$

with the observation date $d = MJD - 55400$ and the source flux $f = log_{10}flux[e^-]$. The MJD

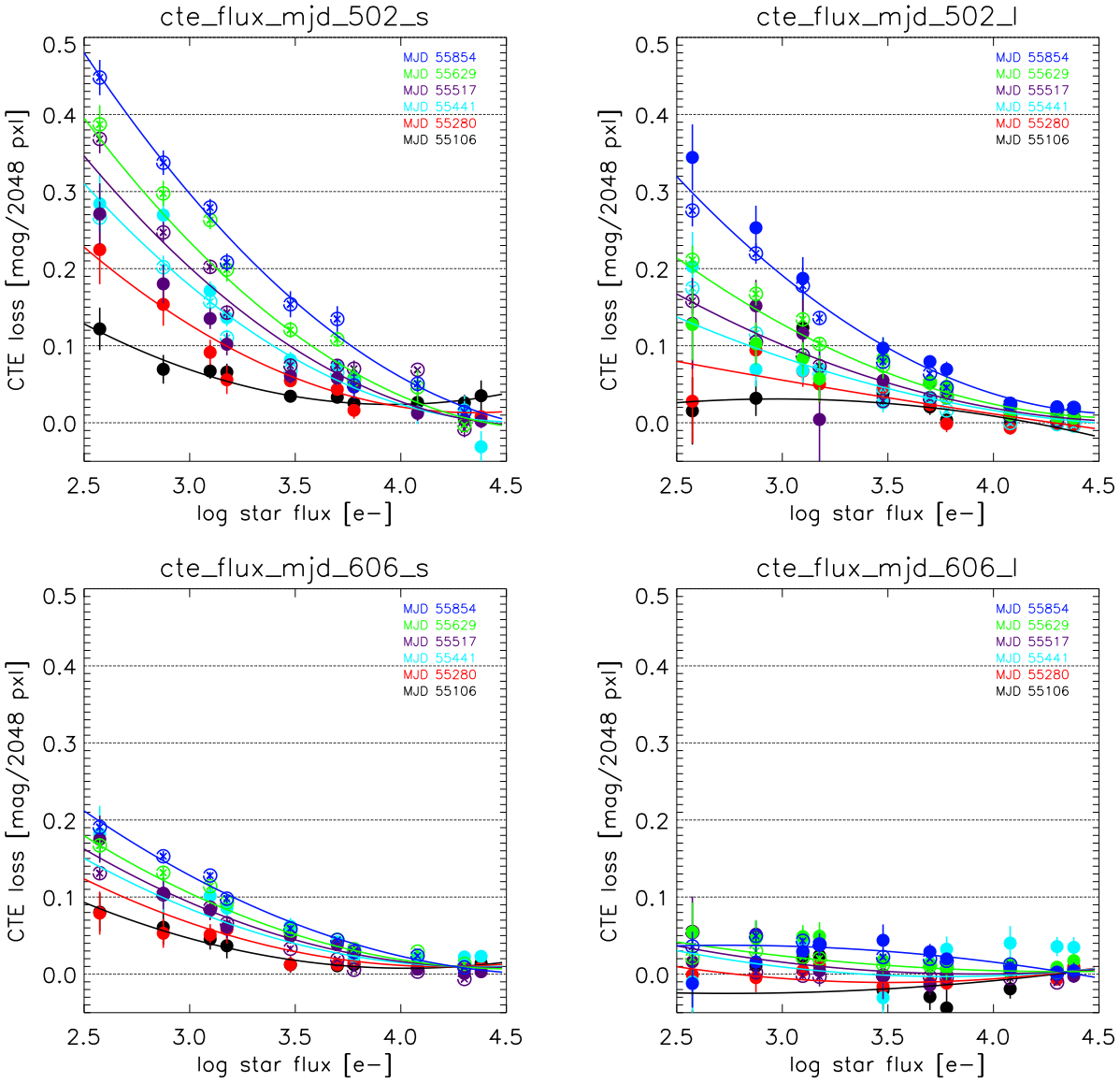

Fig. 4.— CTE loss slope in magnitudes per 2048 detector rows vs log of stars' fluxes, measured in $r = 3$ pixel apertures. Symbol colors refer to the MJD of each calibration observation, from black (lowest losses, earliest dates) to blue (highest losses, most recent dates). Filled symbols represent the sparse cluster NGC6791, open symbols the higher source density field in 47 Tuc/NGC104. Top left: F502N (low background), short exposures; top right: F502N, long exposures. Bottom left: F606W (high background), short exposures; bottom right: F606W, long exposures. The colored lines show the CTE correction model (Equations 2 and 3), fitted to all data points in the respective plot panel (all flux bins, all epochs) simultaneously.

zeropoint was set in the middle of our MJD range, not at the beginning, to reduce the leverage of outlying data points.

The flux correction for an individual source is then given by

$$f_{\rm corr}[mag] = f_{\rm uncorr}[mag] - S\frac{Y}{2048} \tag{4}$$

where S is obtained from equation 2 and Y is the source distance from the amplifier in detector rows.

The coefficients c_{ij} are listed in Table 1, for aperture photometry obtained in aperture radii of 3 pixels. Updated coefficients of the model, and for photometry in larger apertures, will be published on the UVIS CTE website as we include forthcoming calibration data into our analysis. After an initial model fit, outlier data points with a data-to-model difference of 2σ data scatter around the model were removed and the model refitted. The final scatter of the data points around the model is ~ 0.01 mag rms in all panels of Figure 4. We advise caution when using this model to correct sources with observed fluxes much lower than the range shown in Figure 4, since we cannot be sure that the fits can be extrapolated to arbitrarily low fluxes.

The model was fitted for each observational setup - long and short exposures, F502N and F606W filters, individually. We currently only have data for three background levels - 0, 2-3 and 20-30 electrons per pixel, which do not allow us yet to obtain a robust background dependence for the CTE corrections. CVZ observations including varying Earth shine, attempted during Cycle 18, have unfortunately not provided the finer-stepped sky background data that would allow a smooth modeling of the CTE's background dependence; we are scheduling a different approach to such data in Cycle 19. Observers are encouraged to use the correction model for the background level closest to their data, or to cautiously interpolate. The same is true for the CTE dependence on the exposure times, for which we currently only have two data points, and which we expect to depend on the source density of the image to be corrected.

configuration	F502W, short	F502W, long	F606W, short	F606W, long
background $[e^-]$	~ 0	~ 0	$2-3$	$20-30$
c_{00}	1.44358e+00	4.89403e-01	7.63656e-01	2.86341e-01
c_{01}	1.84953e-03	2.19209e-03	4.92893e-04	1.78017e-04
c_{02}	-1.22769e-06	-2.69032e-08	-2.20093e-07	-2.09480e-06
c_{10}	-6.38076e-01	-1.94178e-01	-3.49022e-01	-1.56858e-01
c_{11}	-6.82433e-04	-1.04463e-03	-1.54788e-04	-5.95706e-06
c_{12}	5.60995e-07	1.56760e-07	1.12447e-07	1.13626e-06
c_{20}	7.06972e-02	1.88753e-02	4.03970e-02	2.11097e-02
c_{21}	5.68179e-05	1.26167e-04	9.20672e-06	-7.93585e-06
c_{22}	-5.63594e-08	-3.50145e-08	-1.44093e-08	-1.51143e-07

Table 1: Coefficients for the empirical CTE correction model, given for the four different observational configurations (long and short exposures, F502N and F606W filters) described in this document.

6. Conclusions

We have investigated the evolution of the charge transfer efficiency (CTE) of the WFC3/UVIS detectors over a 2-year period starting 5 months after the WFC3 installation, ranging from October 2009 to October 2011. Using observations of calibration fields in the star clusters NGC6791 and NGC104/47 Tuc, we find a strong evolution of the CTE, amounting to more than 0.1 mag CTE loss per year for stars with a total flux of 1000 electrons, at large distances from the readout amplifiers, in short-exposure zero sky background images. These maximum possible CTE losses for such stars have reached 0.3 mag (24%) as of October 2011 within 3 pixel radius apertures. For even fainter stars around 300 electrons, these losses can reach 50%.

The CTE degradation and associated losses decrease for increasing source fluxes, and for higher sky background levels which partially fill the detector charge traps during readout and lower the losses suffered by the science sources. Already a low background of 2-3 electrons per pixel significantly lowers CTE losses, while a 20-30 electron per pixel background in longer-exposure broadband images brings CTE losses to few percent for sources ranging from few 100 to 10s of 1000s of electrons. We also see significantly lower CTE losses in longer (approx. 350 seconds) exposures than in shorter ones (30-60 seconds), most likely because the larger total charge collected in longer images has a similar, yet non-uniformly distributed trap-filling effect as a higher sky background.

We present an empirical polynomial model that corrects CTE losses as a function of observation date, source flux, and source distance on the detector from the readout amplifiers. The model coefficients are given for low and high backgrounds and long and short exposures separately, while we collect further calibration data to include a smooth parameterization of the latter parameters.

7. Updates and Future Work

Updates of the UVIS CTE evolution and empirical model will be published on the UVIS CTE webpage (`http://www.stsci.edu/hst/wfc3/ins_performance/CTE/`) as new data become available.

Forthcoming updates will include CTI effects on point source photometry in different aperture radii, and errors of CTE slope measurements will be lowered by an improved correction for cosmic ray affected sources. As we process additional calibration data, we will be able to parameterize the dependence of CTI effects on exposure times, source density in the calibration field, and background levels. Finally, we have evidence for *serial* CTI, affecting sources depending on their detector X coordinate, introduced by charge traps in the serial register. Effects of serial CTI are much smaller than the CTI in detector Y direction that is discussed in the current document, and will be the subject of a future study.

A separate document will quantify the moderation of CTI effects by charge injection and the associated noise and image data quality penalties.

References

Anderson, J. & Bedin, L. R. 2010, PASP, 122, 1035
Baggett et al., Jan 2011, WFC3 UVIS CTE Whitepaper
http://www.stsci.edu/hst/wfc3/ins_performance/CTE/cte.pdf

Bushouse et al., Jan 2011, WFC3-ISR-2011-02: WFC3/UVIS Charge Injection Behavior: Results of an Initial Test. H. : http://www.stsci.edu/hst/wfc3/documents/ISRs/WFC3-2011-02.pdf

Casadio, S. & Arino, O. 2011, Advances in Space Research, 48, 1056

Chiaberge, M., Lim, P.-J., Kozhurina-Platais, V., Sirianni, & Mack, J., ACS ISR 2009-01

Fürst, F., Wilms, J., Rothschild, R.E., et al. 2009, Earth & Planetary Science Letters, 281, 125

Giavalisco, M., Mar 2003, WFC3-ISR 2003-01: Minimizing CTE losses in the WFC3 CCDs: Post Flash vs. Charge Injection
www.stsci.edu/hst/wfc3/documents/ISRs/2003/WFC3-2003-01.pdf

Khozurina-Platais, Gilliland, Baggett, Feb 2011, WFC3-ISR-2011-06: WFC/UVIS-Cycle 17: CTE External Monitoring - NGC 6791
http://www.stsci.edu/hst/wfc3/documents/ISRs/WFC3-2011-06.pdf

Massey, R. 2010, MNRAS, 409L, 109

Mewaldt, R. A.,Davis, A. J., Lave, K. A., et al. 2010, ApJL, 723, 1

Noeske, K., Baggett, S., Bushouse, H., Gilliland, R. & Khozurina-Platais, June 2011: WFC3 UVIS CTE and Charge Injection: June 2011 Update for Cycle 19 Observers:
http://www.stsci.edu/hst/wfc3/ins_performance/CTE/UVIS_CTE_Cy19_Update.pdf